

Transient large-scale dynamos in supernova progenitors

Eric G. Blackman,^{1,2,3} Jason T. Nordhaus,^{1,2} John H. Thomas^{1,3,4}

1. Dept. of Physics and Astronomy, Univ. of Rochester, Rochester, NY 14627, USA; 2. Laboratory for Laser Energetics, Univ. of Rochester, Rochester, NY 14623, USA; 3. Isaac Newton Institute for Mathematical Sciences, Univ. of Cambridge, Cambridge CB3 0EH; 4.

Dept. of Mechanical Engineering, Univ. of Rochester, Rochester, NY 14627, USA

(submitted to MNRAS)

ABSTRACT

Observational evidence for anisotropy in supernovae (SN) and the association with jetted sources like gamma-ray bursts have revived considerations of the role magnetohydrodynamic outflows might play therein. Understanding how dynamos might operate in supernova progenitors is therefore of interest. Here we study a large scale dynamo for the conditions of a rapidly rotating neutron star surrounded by a convective envelope. Large scale interface dynamos have been studied for the Sun, naked white dwarfs, and post-AGB stars where strong shear layers are surrounded by convective envelopes. Because shear in SN progenitors is due only to the initial collapse and not rejuvenated by convection, we include the dynamical evolution of the shear as it responds to field growth, and show that the dynamo is transient. Our transient dynamo provides estimates of large-scale poloidal and toroidal fields, whose product determines the Poynting flux. The poloidal magnetic field is much weaker than the toroidal field, and the actual Poynting flux is lower than estimates which invoke the magnitude of the magnetic energy. For a $15M_{\odot}$ progenitor with inner shear layer rotation rates $\sim 200\text{Hz}$, dynamo durations are $5 - 50$ sec and provide up to $\sim 5 \times 10^{50}$ erg from the associated Poynting flux. This may be marginally able to power a SN, and can produce asymmetries and/or pulsar kick velocities, but the mechanism of outflow formation needs more work. A signature of our large scale dynamo is that the Poynting flux oscillates on ~ 1 sec time scales. This highlights the need for observational constraints on the time profile of energy delivery to a SN.

Key Words: supernovae: general – stars: magnetic fields – stars: neutron – MHD – dynamo theory

1. Introduction

Observations suggest that many supernovae (SN) are intrinsically anisotropic. As summarized by Wheeler (2004a,b), the evidence comes from: (1) bipolar structure in supernova remnants (Dubner et al. 2002); (2) optical jet and counter jet structures in Cas A (Fesen 2001); (3) X-ray jets and toroidal emission of intermediate mass elements (Hughes et al. 2000; Hwang, Holt, Petre 2000; Willingale et al. 2002); (4) asymmetric ejecta in SN1987A perpendicular to the major axis of the rings (Pun et al. 2001; Wang et al. 2002); and (5) Optical polarization in both Type I and Type II supernovae with the Type Ib,c polarization being higher than that of Type II (Wang et al. 2001), but with the latter increasing with time (Leonard et al. 2000, 2001). Since Type I SN represent a naked core, and the core at late times in Type II becomes exposed, a consistent interpretation is that the very engine of the SN is a source of this asymmetry.

At minimum, anisotropy likely reveals the role of rotation in SN engines and the need to incorporate non-spherically symmetric physics. The combination of rotation, highly ionized plasma, stratified turbulence, and magnetic fields has prompted various considerations of MHD outflows as a source of this asymmetry, if not the source of the SN explosion itself. Recent renewed interest in proposals relating MHD outflows to supernovae (Leblanc & Wilson 1970; Meier et al. 1976; Ardeljan, Bisnovatyi-Kogan, & Moiseenko 1998; Khokhlov et al. 1999; Wheeler et al. 2000; Wheeler, Meier, & Wilson 2002; Moiseenko, Bisnovatyi-Kogan, & Ardeljan 2004) is bolstered by the observational association of SN with Gamma-ray bursts (Galama et al 1998; Iwamoto et al. 1998; Stanek et al. 2003; Hjorth et al. 2003; Thomsen et al. 2004; Cobb et al. 2004 Gal-Yam et al. 2004; Malesani et al. 2004). MacFadyen, Woosley, & Heger 2001). That magnetized outflows have also long been thought to be important in young stellar objects, active galactic nuclei, pulsar winds, and microquasars (of which GRB are likely one class) suggests that explosive outflows in astrophysics could all involve some combination of rotation and magnetic fields.

Previous work on magnetic field amplification in pre-supernovae core conditions have employed either (i) simple shear that grows toroidal field linearly (e.g. Leblanc & Wilson 1970; Ardeljan, Bisnovatyi-Kogan, & Moiseenko 1998; Wheeler 2000), (ii) traditional kinematic convective $\alpha - \Omega$ dynamo models to grow ordered fields (Thompson & Duncan 1993), which in principle grow large-scale fields exponentially, or (iii) the exponential field growth from the magneto-rotational instability (MRI, e.g. Balbus & Hawley 1998) (Akiyama et al. 2003; Moiseenko et al. 2004), whose saturated magnetic energy was used as a rough estimate for the large-scale toroidal field. Each has its merits and its limitations. In the presence of turbulent diffusion, (i) will not sustain the field. The approach of (ii) offers exponential growth and is an important step forward, but the backreaction of the

field on the driving flow, the separate generation of toroidal vs. poloidal fields, and the spatial location of the α and Ω effects still needs to be determined. The recent approach of Akiyama et al. in (iii) offers a useful model of the internal and rotational structure of the inner SN engine, and also makes careful estimates of the saturated energy of the magnetic field adopted from results obtained in MRI disk simulations. Whether these values also apply to pressure-supported stars remains to be studied in detail because the MRI likely transports angular momentum on spherical shells (Balbus & Hawley 1994), not radially. The latitudinal differential rotation may be most important. If 3-D turbulence develops, then field amplification will take place from the MRI. Moiseenko et al. (2004) provide 2-D simulations of what appear to be MRI-driven SN, starting from a relatively strong, ordered poloidal field. However, in 2-D, there is no sustained dynamo action to amplify the total magnetic energy from arbitrarily small values.

An important question is whether a magnetically driven outflow requires a large-scale field in the supernova progenitor engine. By large-scale field, we mean one that maintains the sign of its flux over many dynamical times, when averaged over the size of the region. Large-scale fields are helpful, if not necessary, in generating outflows in disks or stellar coronae, and perhaps by analogy, also in a SN engine. If the field needs to buoyantly rise above the dynamo region to a height at which it provides the dominant contribution to the stress, the field should be of large enough scale to avoid being shredded by turbulence. Once at the region where it dominates, the field can further relax to even larger scales. Comparing the shapes of observed outflows to those from theoretical studies (e.g. Moiseenko et al. 2003) may help determine the relative importance of large scale fields vs. a simple magnetic pressure gradient.

By incorporating differential rotation, turbulence, and ionized plasma, one would ultimately like to understand the physics of the proto-supernova engine, independent of what is needed. With this in mind, we study large-scale magnetic field growth. Large-scale field generation does not exclude the presence of the MRI. When the MRI operates in a stratified medium, it may provide a source of helical turbulence that allows one sign of magnetic helicity to migrate to large scales, producing large-scale magnetic fields (e.g. Brandenburg et al. 1995; Blackman & Tan 2004) or a helicity flux (Blackman & Field 2000; Brandenburg & Cho 2001). In our large scale dynamo, the source of helical turbulence is considered to be convection driven by neutrino deposition rather than the MRI. It should be emphasized that studies focusing on magnetic energy amplification from the MRI (Balbus & Hawley 1998) typically focus on the total magnetic energy (e.g. Akiyama et al. 2003) rather than a large-scale field in the sense we have defined above. It should also be noted the backreaction of the field on the shear is not usually considered in MRI studies.

Here we consider a dynamical generalization of the large-scale interface dynamo proposed by Parker (1993) for the Sun (see also Charbonneau & MacGregor 1997; Markiel & Thomas 1999; Zhang et al. 2003). Our results are not too sensitive to the fact that our dynamo is of the interface type, but it should be noted that interface dynamos differ from the original $\alpha - \Omega$ dynamos in that the dominant region of shear and the dominant region of helical turbulence are not co-spatial. The shear associated with differential rotation is concentrated in a layer (the Ω -layer) lying beneath the turbulent convection zone (the α layer). Such a scenario has been a leading model for the solar dynamo, and has also been applied to white dwarfs (Markiel, Thomas & Van Horn 1994; Thomas, Markiel & Van Horn 1995) and to AGB stars (Blackman et al. 2001). In all of these cases, helical turbulence in the convective zone provides the dynamo α effect and thus generates the poloidal field. Asymmetric turbulent pumping (e.g. Tobias et al. 2001) pushes the poloidal field downward into the strong shear layer where the toroidal field is amplified. The rotational and convective structure of the proto-supernova engine in core-collapse supernovae has a similar structure, with a strong shear layer surrounded by a convective envelope. However, unlike the Sun where the small differential rotation is reseeded by convection, in the SN context the shear decays dynamically as the field grows. We therefore explicitly include the dynamical evolution of the shear and rotation in addition to that of the magnetic field, unlike previous work. The dynamo becomes transient in the SN progenitor context.

Dynamo research must accommodate two competing needs: the need for a theory that rigorously includes the backreaction of the growing magnetic field on the flow, and the need to model the field growth in a realistic system. Meeting these two goals is difficult both analytically and numerically, and compromises must be made. Our aim here is to develop a transient large scale dynamo model and apply it to the SN progenitor context as simply as possible, while still including the time-dependent nonlinear dynamical quenching of the differential rotation by the magnetic field growth.

In section 2 we present the transient dynamo model. In section 3 we discuss the parameter choices and present the corresponding solutions to the dynamo equations. In section 4 we discuss the implications of the calculated Poynting flux. We conclude in section 5 and identify some unresolved issues for future work.

2. Local interface dynamo equations

We generalize the interface dynamo model of Markiel, Thomas & Van Horn (1994) to include the dynamical backreaction on shear and rotation from the amplified magnetic field and Poynting flux. The structure of the basic model is illustrated in the meridional

slice shown in Fig. 1. Two distinct regions adjoin at the interface radius $r = r_c$. In the inner region, the differential rotation (the Ω effect) wraps the poloidal field into a toroidal field with the rotation profile initially varying linearly from Ω at $r = r_c$ to $\Omega + \Delta\Omega$ at $r = r_c - L$, with $\Delta\Omega = f\Omega$, where f is a dimensionless fraction. The values of the quantities at the initial time of the calculation are indicated by a subscript 0, that is f_0 , Ω_0 , and $\Delta\Omega_0$. The outer layer, representing the convection zone, rotates rigidly with angular velocity Ω_0 . There, cyclonic convection (the α -effect) converts toroidal field into poloidal field. This poloidal field is then pumped or diffused downward into the Ω layer where the shear again further amplifies the toroidal field. The relevant α layer has scale height L_c , which corresponds to a density scale height from the base of the convection zone. A full treatment of the interface dynamo would include anisotropic diffusion, stratification and shear, a global 3-D treatment of the convection, a fully self-consistent role of buoyancy, a self-consistent sustenance of α magnetic field on the velocity field. We provide a minimalistic approach to demonstrate the mechanism simply.

To solve for the magnetic field, we employ the mean-field induction equation, derived by averaging the induction equation in the presence of helical velocity fluctuations. The standard mean field induction equation, ignoring cross-helicity, is (e.g. Parker 1979)

$$\partial_t \bar{\mathbf{B}} = \nabla \times \langle \mathbf{v} \times \mathbf{b} \rangle + \nabla \times (\bar{\mathbf{V}} \times \bar{\mathbf{B}}) + \lambda \nabla^2 \bar{\mathbf{B}} = \nabla \times (\alpha \bar{\mathbf{B}}) + \nabla \times (\bar{\mathbf{V}} \times \bar{\mathbf{B}}) - \nabla \times (\beta \nabla \times \bar{\mathbf{B}}) + \lambda \nabla^2 \bar{\mathbf{B}}, \quad (1)$$

where $\bar{\mathbf{B}}$ is the mean field, $\bar{\mathbf{V}}$ is the mean velocity, λ is the turbulent diffusivity, and the turbulent electromotive force is $\langle \mathbf{v} \times \mathbf{b} \rangle = \alpha \bar{\mathbf{B}} - \beta \nabla \times \bar{\mathbf{B}}$, where α is the pseudoscalar helicity dynamo coefficient and β is the scalar turbulent magnetic diffusivity. Although we have in mind a spherical system, for present purposes we simplify the analysis by working in local Cartesian coordinates. Simplified versions of the equations we invoke for the mean magnetic field have been used in previous interface dynamo models (Robinson and Durney (1982), Markiel, Thomas, & Van Horn (1994)) without adequate derivations, and so we present a full derivation here. The coordinates are shown in Fig. 1. Writing $\bar{\mathbf{A}} = (\bar{A}_x, \bar{A}, \bar{A}_z)$ and assuming that (i) the mean fields are axisymmetric (i.e. $\partial_y \bar{\mathbf{Q}} = 0$ for any mean quantity $\bar{\mathbf{Q}}$), (ii) $\bar{\mathbf{V}} = (0, \bar{V}, u)$, (iii) $\bar{\mathbf{B}} = (0, \bar{B}, \partial_x \bar{A})$ (so $\partial_z \bar{A} = 0$) (iv) β is independent of position, and (vi) $\beta \gg \lambda$, we can write the equations for the toroidal magnetic field \bar{B} and the vector potential \bar{A} as

$$\partial_t \bar{B} = -\alpha \partial_x^2 \bar{A} - \partial_z \alpha \partial_x \bar{A} + \partial_x \bar{A} \partial_z \bar{V} - u \partial_z \bar{B} - u \bar{B} / L + \beta \nabla^2 \bar{B} \quad (2)$$

$$\partial_t \bar{A} = \alpha \bar{B} + \beta \partial_x^2 \bar{A}, \quad (3)$$

where we have used $-\bar{B} \partial_z u \sim -u \bar{B} / L$ which we take as a loss term due to magnetic buoyancy with $u > 0$. If we assume that the Fourier transform of the field is proportional to a δ function in wavenumber (i.e. the mean field has a single large scale), then we can

write $\overline{A} = A(t)e^{(ik_xx+ik_zz)}$ and $\overline{B} = B(t)e^{(ik_xx+ik_zz)}$, where $A(t)$ and $B(t)$ are complex-valued functions. Then, assuming the $\partial_z\alpha$ term to be small, Eqs. (2) and (3) become

$$\partial_t B \simeq \alpha k_x^2 A + ik_x r_c A \frac{\Delta\Omega}{L} - i u k_z B - u B / L - \beta k^2 B \quad (4)$$

$$\partial_t A = \alpha B - \beta k^2 A, \quad (5)$$

where $k^2 = k_x^2 + k_z^2$, and we have used

$$\partial_z \overline{V} \sim r_c \Delta\Omega / L \quad (6)$$

to obtain the third term in (4), based on the interface geometry shown in Fig. 1. For the turbulent diffusivity, we write

$$\beta = c_\beta v_1 L, \quad (7)$$

where c_β is a dimensionless constant which can be thought of as $\sim 1/3$ times the ratio of a turbulent fluctuation scale to L , and v_1 is a typical convective velocity at the middle of the α layer (i.e. at $r = r_c + L_1/2$, see Fig. 1). In interpreting $-\frac{uB}{L}$ as the rate of loss of toroidal flux due to the buoyant rise of toroidal flux out of the dynamo region, we use the expression for the rise velocity of a flux tube (Parker 1955, 1979), namely

$$u = \frac{3q}{8} \left(\frac{a}{L} \right)^2 \frac{|\overline{B}|^2}{4\pi\rho v} = \frac{3q}{32} \frac{\overline{V}_A^2}{v}, \quad (8)$$

where a is the radius of the flux tube (assumed to be $L/2$), \overline{V}_A is the Alfvén speed associated with \overline{B} , and $0 < q < 1$ is a dimensionless constant.

2.1. Quenching of α

While there is no compelling evidence that β is quenched in convective 3-D MHD turbulence, recent work on dynamo theory has shown that α quenching can be understood dynamically via magnetic helicity conservation (e.g. Blackman & Field 2002; Brandenburg & Subramanian 2004 for a review). The build-up of the large-scale field is associated with a build-up of the large-scale magnetic helicity, $\overline{\mathbf{A}} \cdot \overline{\mathbf{B}}$. In the absence of boundary terms, magnetic helicity is well conserved, so the small-scale helicity builds up equal and opposite to that of the large scale. Since α depends on the difference between kinetic and current helicities, the build up of small-scale magnetic (and thus current) helicity eventually saturates the dynamo. If boundary terms can remove both small and large-scale helicity (Blackman & Field 2000) then the α quenching is alleviated but at the expense of a lower saturated mean field (Blackman & Brandenburg 2003). If the small-scale helicity can be

preferentially removed then the large-scale growth proceeds longer to larger values. Shear may also reduce the impact of α quenching (Brandenburg & Sandin 2004). Shear also leads to anisotropic turbulence and possibly a shear-current dynamo (Rogachevskii & Kleeorin 2003), though we do not presently discuss this further.

Here we are mainly interested in demonstrating the plausibility of a transient large scale dynamo and adopt a parameterization of the α effect backreaction that can be used to approximate the non-linear quenching. The quenching formula used for previous interface dynamos (Markiel, Thomas, & Van Horn (1994)) provides an adequate local approximation, namely

$$\alpha = \alpha_0 \text{Exp} \left[-\gamma_1 \frac{\bar{B}^2 / 8\pi}{\rho_1 v_1^2 / 2} \right], \quad (9)$$

where γ_1 is a dimensionless constant, ρ_1 and v_1 are the mass density and a typical convective velocity at the middle of the α layer, and (Durney & Robinson (1981))

$$\alpha_0 = c_\alpha \frac{L_1^2 \Omega_0}{r_c}, \quad (10)$$

where $c_\alpha < 1$ is a dimensionless constant.

2.2. Quenching of $\Delta\Omega$ and Ω

The primary source of energy for the interface dynamo is differential rotation and since this is supplied only by the initial rotation profile, the amplification of the field will drain this energy. A crude approximation would be to simply estimate the spin down time of the shear layer and ask only that the dynamo operate over that period without incorporating dynamical backreaction equations for the shear and rotation. This however, gives only an upper limit on how much energy the dynamo would actually produce. We opt for a somewhat better approach: to derive approximate dynamical equations for the shear and rotation and incorporate them into the dynamo theory.

To obtain an expression for quenching of the differential rotation by the magnetic field, we recall that $\Delta\Omega = f\Omega$, where f is the fractional change of rotation across the Ω layer. Both f and Ω are functions of time so we need two differential equations. Instead of equations for f and Ω , we can alternatively derive equations for the evolution of $\Delta\Omega$ and Ω as the dependent variables.

If we ignore second derivatives in space, using (6) we can write the differential equation for the shear at $r = r_c$ as

$$\partial_t(r_c \Delta\Omega) = \partial_t(\bar{V}_y(r_c) - \bar{V}_y(r_c - L)) \simeq \partial_t(L \partial_x \bar{V}_y). \quad (11)$$

Thus, to obtain the desired differential equation for the right hand side, we subtract the time dependent differential equations for the velocity at r_c and $r_c - L$. From the Navier-Stokes equation and the assumption that gradients in the y direction vanish, we have,

$$\partial_t \bar{V}_y = -\bar{\mathbf{V}} \cdot \nabla \bar{V}_y + \frac{1}{4\pi\rho} (\bar{\mathbf{B}} \cdot \nabla) \bar{B}_y \simeq \frac{1}{4\pi\rho} \partial_x \bar{A} \partial_z \bar{B}_y, \quad (12)$$

since the dominant backreaction arises from the magnetic field. Note that pressure gradients do not contribute because y -gradients vanish in our approximation. From Eqs. (11) and (12) we then have

$$\begin{aligned} \partial_t(r_c \Delta \Omega) &= \frac{1}{4\pi\rho} \partial_x \bar{A} \partial_z \bar{B}_y|_{r_c} - \frac{1}{4\pi\rho} \partial_x \bar{A} \partial_z \bar{B}_y|_{r_c-L} \simeq \frac{L}{4\pi} \partial_z \frac{1}{\rho} \partial_x \bar{A} \partial_z \bar{B}_y \\ &= \frac{L}{4\pi} \left[\frac{1}{\rho} (\partial_z \partial_x \bar{A} \partial_z \bar{B}_y)_{r_c} + (\partial_x \bar{A} \partial_z^2 \bar{B}_y)_{r_c} - \left(\frac{\partial_z \rho}{\rho^2} \partial_x \bar{A} \partial_z \bar{B}_y \right)_{r_c} \right]. \end{aligned} \quad (13)$$

In our simple model we take $\partial_z \rho \sim (\rho_2 - \rho_1)/L$. Using $\bar{A} = A(t)e^{i(k_x x + k_z z)}$ and $\bar{B} = B(t)e^{i(k_x x + k_z z)}$ as in the derivation of Eqs. (4) and (5), we then obtain

$$\partial_t \Delta \Omega = \frac{L}{4\pi r_c \rho} \left[-k_x k_z^2 \rho (Re(\bar{A}) Re(i\bar{B}) + Re(i\bar{A}) Re(\bar{B})) - \partial_z \rho k_x k_z Re(i\bar{A}) Re(i\bar{B}) \right]. \quad (14)$$

As stated above, we also need an equation for the time evolution of $\Omega(t)$. We obtain this equation by noting that the rotational energy of the field-anchoring matter is drained by the Poynting flux. The Poynting flux at r_c is given by

$$L_{mag} = \frac{c}{4\pi} \int \bar{\mathbf{E}} \times \bar{\mathbf{B}} \cdot d\mathbf{S}_c \simeq \frac{1}{4\pi} \int \Omega r_c Re(\bar{B}_z) Re(\bar{B}_y) \cdot d\mathbf{S}_c \simeq Re(\bar{B}_z) Re(\bar{B}_y) \Omega r_c^3. \quad (15)$$

Calculating this quantity requires the separate determination of the toroidal and poloidal magnetic fields: because these components can be out of phase, the maximum Poynting flux is not simply the product of their respective maxima. We approximate the available rotational energy as the kinetic energy associated with a region of length L rotating with a uniform rate of $\frac{\Omega + f\Omega}{2}$. That is $E_{rot} \sim \frac{1}{2}ML^2\left(\frac{\Omega + f\Omega}{2}\right)^2$, where $M \simeq 10^{34}\text{g}$ is the mass of the shear layer. Using these relations and (15), the time derivative of the rotational energy then leads to the time-evolution equation for Ω , in the form

$$\partial_t \Omega \simeq \frac{Re(\bar{B}_x) Re(\bar{B}_y) r_c^3}{\frac{1}{2}ML^2\left(\frac{\Omega + f\Omega}{2}\right)^2} - \partial_t \Delta \Omega. \quad (16)$$

Eqs. (16), (14), (4) and (5) are the coupled differential equations to be solved for the transient large scale interface dynamo.

3. Discussion of Solutions

3.1. Kinematic Solution

For the relevant parameters, the first term on the right of (4) is small compared to the next term, implying that we are initially in the $\alpha - \Omega$ interface dynamo regime. It is useful to first consider the kinematic limit, $\gamma_1 = q = 0$, $\partial_t f = \partial_t \Omega = 0$, which allows us to determine the conditions for initial growth of the dynamo field. In this case, (4) and (5) are the only equations to be solved. Assuming that $k_z \ll k_x$, there are then exponentially growing solutions of the form $A(t) = A_0 e^{nt}$ and $B(t) = B_0 e^{nt}$, such that $\bar{A} = \text{Re}(A_0 e^{nt+ikx})$ and $\bar{B} = \text{Re}(B_0 e^{nt+ikx})$, and

$$\text{Im}(n) = \left(\frac{\alpha_0 \Delta \Omega k r_c}{2L} \right)^{1/2}. \quad (17)$$

The amplitude of these waves grows (i.e. $\text{Re}(n) > 0$) only when the dynamo number

$$N_D \equiv \frac{\alpha_0 k r_c \Delta \Omega_0}{2L \beta^2 k^4} \quad (18)$$

exceeds unity. This kinematic solution will provide insight into the non-linear solutions.

3.2. Nonlinear Dynamo Solutions for SN Progenitors

For the engine structure, we employ the profiles of Akiyama et al. (2003) for a rapidly rotating neutron star (NS) formed from the collapse of a $15 M_\odot$ progenitor. These authors used a 1-D stellar evolution code to obtain the radial structure of a spherical core collapse, and then computed the rotational velocity profiles *a posteriori* by assuming that angular momentum is conserved on spherical shells during the collapse. We adopt the values of the density and rotation profiles corresponding to 384 milliseconds after bounce. While Akiyama et al. (2003) used their structure and rotation solutions as inputs for their MRI dynamo calculations, we use these inputs for the interface dynamo of the previous section.

Using the characteristic numbers, our differential rotation layer (Ω -layer, Fig. 1) extends down to the surface of the NS ($r_c - L = 1.5 \times 10^6$ cm) and the base of the convection zone is located at $r_c = 4 \times 10^6$ cm. We take the α effect to occur above the base of the convection zone in a layer whose thickness ($L_1 = 2.3 \times 10^6$ cm) equals the local density scale height. The density in the middle of the Ω layer is taken to be $\rho_2 = 2.4 \times 10^{13}$ g/cm³ and that of the α -layer is taken to be $\rho_1 = 2.4 \times 10^{12}$ g/cm³ (Akiyama et al. 2003). A typical convective velocity (e.g. Herant et al. 1994) of $v_1 = 10^8$ cm/s is taken in the middle of the α layer and is sustained by the neutrino luminosity and lepton gradients. The interface

dynamo equations of the previous section contain the dimensionless constants γ_1 , c_β , c_α , and q . For the α quenching parameter, γ_1 , we take $\gamma_1 = 0.1$, for which the solutions turn out to be Ω -quenching limited. Regarding the parameters c_β , c_α , and q , we note that the dynamo number is sensitive only to the ratio c_α/c_β^2 , whereas q enters in the buoyancy loss term and c_α enters in the kinematic dynamo frequency. A range of choices can be considered to be appropriate given the uncertainty in the detailed properties of the turbulence, but, in the spirit of mixing-length theory, we choose $c_\beta = 0.06$, $c_\alpha = 0.002$, and $q = 0.005$, which yield dynamo solutions matching the solar dynamo period and field strength when the theory (without Ω and $\Delta\Omega$ quenching) is applied in that context (Markiel, Thomas, & Van Horn (1994)).

The magnetic field strengths $\overline{B}_x, \overline{B}_y$ are computed at the interface layer ($r = r_c$). At $r = r_c$, $x = r_c\theta$ locally where θ is the poloidal angle from the prescribed z axis in Fig. 1. We must choose the mode whose growth we seek. Although the Cartesian approach technically applies only locally, we choose the mode that most closely corresponds to dipole symmetry, namely that for which $k_x r_c = 2$. Fig. 2 shows the poloidal field, toroidal field, and Poynting flux vs. time for values of $\Omega_0 = 160, 200\text{Hz}$ and $f_0 = 0.7, 0.6$ respectively. For the same combinations of Ω_0 and f_0 , Fig. 3 shows the total rotational energy of the shear layer, the differential rotation $f\Omega$, and rotation Ω at r_c . Figs. 4 and 5 are analogous to Figs. 2 and 3 but for $\Omega_0 = 160, 200\text{Hz}$, and $f_0 = 0.5, 0.3$, respectively. γ_1 . The figures illustrate the transient nature of the dynamo.

For the parameters of interest, both the saturation and transient nature of the dynamo are due to f and Ω quenching. In the absence of shear quenching, it would be α quenching that determines the maximum amplitudes of the field and Poynting flux. If α quenching were dominant before Ω quenching kicked in, then the curves of Fig. 2 and 4 would instead incur a “flat top” region in which the peak amplitudes during the cycles remained constant over an intermediate duration before decaying. The fact that the amplitude peaks rise and decay without a flat top indicates that the system is $f\Omega$ -quenching limited. Were the backreaction of the field on the shear not included, or were the differential rotation and rotation constantly being reseeded, the field and the Poynting flux would asymptote to an oscillating solution of constant peak amplitude.

Increasing f_0 and Ω_0 increases the initial dynamo number N_D . This increases the rate of growth and maximum value of the fields obtained, as can be seen by comparing the peak values in respective columns of Figs. 2 and 4. However, due to the finite amount of rotational energy, estimated above (16), a faster growing dynamo lasts a shorter time. This can also be seen by comparing Figs. 2 and 4: the first and second columns of Fig. 2 have larger initial dynamo numbers than the first and second columns of Fig. 4 respectively,

since only f_0 changes between the two sets of plots.

Figs. 3 and 5 show that, during the phase in which the dynamo is active, the rotational energy drops by a factor ~ 5 . That Ω and $f\Omega$ do not fall to 0 indicates that the effective dynamo becomes sub-critical well before all of the rotational energy is drained. The notches that occur in the decay of these rotational quantities occur during the phase of each cycle when the field is well away from its peak in amplitude. During this phase, the damping of the differential rotation and rotation is weak, and their rapid decay is arrested. Note that the Poynting flux drops below zero during part of the field oscillations (see the top panels in Figs. 2 and 4), and so the rotational quantities even slightly increase during that time as seen in Figs. 3 and 5. This effect is small and for the most part the curves represent decay to the values at which the dynamo number drops below the critical value for growth.

The oscillation periods of the toroidal and poloidal field in Figs. 2 and 4 are roughly consistent with $2\pi/Im(n)$, (the inverse of the kinematic dynamo frequency of Eq (17)) at early times until the rise to the first maximum peak. During this time, the Poynting flux oscillates with a period half that of the these field components. After the field and Poynting flux rise to their absolute maxima, the cycle period increases slightly. This modest increase occurs because the cycle period in Eq. (17) is $\propto \Omega^{-1/2}\Delta\Omega^{-1/2}$, and the dynamical quenching of $\Delta\Omega$ and Ω thus increase the period. However, only a modest decrease in $\Omega\Delta\Omega$ makes the dynamo number subcritical, after which the field decays; thus a large increase in dynamo period is not expected. Note also that α quenching is not expected to play a large role in the evolution of the cycle period because α quenching kicks in when the field satisfies $|B| \sim |B_\phi| \sim 10^{15} \left(\frac{\rho_1}{2.4 \times 10^{12} \text{ g/cm}^3}\right) \left(\frac{v_1}{10^8 \text{ cm/s}}\right)^2 \left(\frac{\gamma_1}{0.1}\right)^{-1} \text{ G}$. In the present case, the field amplitude is not limited by α quenching, as discussed above. Even if the differential rotation and rotation were reseeded and the amplitude was limited by α quenching, the field would approach its maximum only for a small fraction of the cycle.

If signatures of the time dependence of energy injection to SN could be constrained observationally, the quasi-periodicity seen in the Poynting flux would be a specific prediction of a large-scale dynamo influenced SN. Similarly, were a Poynting-flux driving cycle to operate in GRB progenitors, one might consider this to provide a source of variability.

4. Further Implications

4.1. Energetics and SN Outflows

In Fig. 6, we plot the integrated Poynting flux over the duration of the transient dynamo. The results show that the Poynting flux does extract about 20-30% of the initial

rotational energy available. Typically, values up to 5×10^{50} erg are obtained, which could be modestly increased for larger rotation speeds (but these are beyond the applicability of the structure model adopted from Akiyama et al. 2003). These values might be marginally sufficient to drive the supernova because the binding energy above the core for a $15M_{\odot}$ progenitor is $\sim 5 \times 10^{50}$ erg (Woosley, Heger, Weaver 2002). The calculated Poynting flux is at least sufficient to drive an outflow through the stellar envelope (Wheeler et al. 2000), making the SN anisotropic. This may occur like a “jack-in-the-box” type of magnetic spring explosion. (In addition to Wheeler, Meier, & Wilson (2002), see also Matt et al. (2003) for simulations of a magnetic explosion without specifying the field origin, and Moiseenko et al. (2004) for a magnetic explosion driven SN.).

The potential efficacy of magnetically-driven outflows for SN is evident from recent work by Moiseenko et al. (2004). However, as in the magnetic explosion of Matt et al (2003) for planetary nebulae, Moiseenko et al. (2004) start with a significant large-scale poloidal field, comparable in strength to the saturated poloidal field we grow here from an initially small seed field. Any transient dynamo driven outflow must occur while the dynamo is active because afterward the field decays.

4.2. Pulsar kicks

Suppose that we want to appeal to magnetically driven outflows both for driving a SN and for producing pulsar kick velocities ~ 200 km/s. Too much collimation may be undesirable for SN driving, as an overly collimated jet may simply bore a narrow hole through the envelope without driving the global explosion. At the same time, the stronger the collimation for a given amount of mechanical luminosity, the smaller the asymmetry needed to drive a significant kick. The source of energy for the wind is ultimately rotational energy of the shear layer (or the NS). The fraction which goes into Poynting flux is that which is available for the outflow. It is therefore instructive to estimate the ratio of the kick kinetic energy E_k to that available from our estimated Poynting flux. The ratio for a $1.4M_{\odot}$ neutron star is

$$q = \frac{E_k}{E_{mag}} \simeq 0.01 \left(\frac{v_k}{200 \text{km/s}} \right)^2 \left(\frac{E_{mag}}{2 \times 10^{50}} \right)^{-1} \quad (19)$$

where E_{mag} is scaled to our typical values for the $15M_{\odot}$ progenitor. That $q \ll 1$ is favorable for an asymmetric bipolar outflow to drive the kick because this means only a small asymmetry is required. This also implies that a kick from the magnetically driven bipolar outflow can in principle be accomplished with a much lower field strength than that

associated with the indirect role of magnetic fields in producing a neutrino-driven kick (Lai & Qian 1998).

4.3. No neutron loading, no magnetars, and no contradiction with the MRI

Several other consequences of the interface dynamo in the context of previous work on MHD and field generation in the SN engine deserve mention. First, because the magnetic field in the interface dynamo model is maximized at the base of the convection zone ($r_c - L \leq r \leq r_c$) rather than at the NS radius ($r_{ns} < r_c - L$), the outflow would be less loaded with neutron-rich material than in a model that amplifies the field more strongly at the surface of the NS (Meier et al. 1976). Too much neutron loading by jets emanating from too deep within the engine would produce r -process material in excess of that observed. Second, because the dynamo is transient, once the rotational energy is extracted, the field strength falls well below 10^{15} G as we have shown in Figs. 2 and 4. In this respect, the presence of 10^{15} G fields in the supernova progenitor does not imply an overabundance of magnetars. There is therefore no contradiction between magnetically driven SN associated with pulsars and present surface fields $<< 10^{15}$ G. The strong magnetar surface fields would not be produced by the interface dynamo, but instead perhaps from a dynamo within the NS (Thompson & Duncan 1993) or from a fossil field from an earlier stage that was amplified by flux freezing, and dynamically relaxed during NS formation (Blackman & Field 2004; Braithwaite & Spruit 2004).

The interface dynamo field does not extend beneath $r_c - L$ because there is insufficient convective turbulence between r_{ns} and $r_c - L$ for the field to grow exponentially there. In the absence of another instability such as the MRI, the field would only grow linearly for $r < r_c - L$. Linear growth may have difficulty competing with the buoyant loss of field from this region. In contrast, at r_c , exponential growth in the interface dynamo is facilitated even in the absence of the MRI via the anisotropic downward pumping of the poloidal magnetic field into the shear region (e.g. Tobias et al. 2001).

The interface dynamo does not exclude the possible operation the MRI for $r < r_c - L$. The MRI can in principle produce either a small-scale or a large-scale magnetic field (as defined in section 1), but the latter only when the turbulence resulting from the MRI is helical. It may be that field amplification below $r_c - L$ is in fact due to the MRI and that the pressure gradient resulting from this field plays a role in the SN driver (Akiyama et al. 2003). However, it remains to be understood how effectively the MRI operates from radial shear as a generator of turbulence in pressure-dominated, convectively stable regions of stellar interiors (Balbus & Hawley 1994). Latitudinal rather than radial differential

rotation may be more more important for the MRI in these environments. As in the present calculations, the backreaction of the field on the shear needs to be incorporated in future MRI studies.

Due to the backreaction of the growing field on the shear, the transient nature of any of these dynamos require that outflows are produced during the dynamo’s operation. This requires understanding an essential part of process that we have not focused on here: the mechanism by which the Poynting flux actually produces the outflow. The magnetic stress should be the dominant stress for the outflow to be magnetically driven. While this does not necessarily require that the plasma be dominated by magnetic pressure, it is easier to understand the magnetic stress dominance when the magnetic pressure is dominant. The latter condition is not at all guaranteed in these SN progenitor environments.

5. Conclusion

We have applied a local, transient, $\alpha - \Omega$ interface dynamo model to the proto-supernova engine structures presented in Akiyama et al. (2003). This interface dynamo, like that commonly thought to be operating in the Sun, is a large-scale helical dynamo in which the shear layer providing the Ω effect lies beneath the turbulent convection supplying the helical α effect. For core-collapse proto-supernovae engines, the convection is driven by shock heating and the shear layer beneath it derives from the initial stellar core collapse. Unlike the Sun, the much stronger shear for the SN progenitor comes from the initial collapse and is not readily reseeded by convection. We have therefore developed a nonlinear transient dynamo that includes the dynamical backreaction of the growing field on the shear. We have also included the extraction of rotational energy via Poynting flux. Although we also parameterize α quenching, the quenching of the shear dominates.

The transient dynamo applied to a $15M_{\odot}$ progenitor of maximal inner shear layer rotation rate of 200Hz lasts $\sim 10 - 50$ seconds, leading to large-scale toroidal fields of strength 5×10^{14} G and large-scale poloidal fields of strength $\sim 10^{13}$ G at the base of the convection zone. The poloidal magnetic field has a significantly lower magnitude than the toroidal field, which lowers the peak Poynting flux (which depends on the product of the two field components) compared to previous rough estimates that invoke the magnitude of the magnetic energy (e.g. Wheeler, Meier, & Wilson 2002). The Poynting flux, when integrated over the lifetime of our transient dynamo for these rotation rates (Fig. 6) may be energetically sufficient to drive the SN. Faster rotation rates will do a bit better, but very high rotation rates are beyond the applicability of the structure model we adopted from Akiyama et al. (2003), and the curves of Fig. 6 start to flatten at large Ω_0 . The Poynting

flux can in principle provide asymmetries and a pulsar kick velocity. Because the Poynting flux is transient, any outflow must be driven during the dynamo duration.

Because the large-scale toroidal and poloidal fields are out of phase, the associated Poynting flux oscillates with period ~ 1 sec. We therefore predict that if a SN is driven by a large-scale dynamo rather than a disordered field, then the injection would show ~ 1 sec variability during the injection duration τ_b . Observational constraints on the time scale for SN energy injection are needed.

Our approach differs from the $\alpha - \Omega$ dynamo of Duncan & Thompson (1993) which operates inside the NS, but agrees with the result that the large-scale toroidal field can have a magnitude $\sim 10^{14-15}$ G. Our results are also complementary to the MRI-based estimates of Akiyama et al. (2003), who obtained magnetic energies associated with a 10¹⁵ G field, but inferred these values from turbulent magnetic energy saturation of the MRI turbulence rather than from specific values of a large-scale magnetic field. Also, unlike previous work, we include the backreaction of the field growth on the shear.

A key unresolved issue for any transient dynamo outflow model is determining how the magnetic stress actually drives the outflow, particularly if the magnetic pressure does not dominate the thermal pressure. Self-consistent numerical studies that include both the amplification of a very weak seed field and the outflow generation (Matt et al. 2003; Moiseenko, Bisnovatyi-Kogan, & Ardeljan 2004) warrants development.

Similar dynamo and outflow studies for faster rotating SN progenitors, and for more massive “failed” SN (MacFadyen & Woosley 1999; MacFadyen, Woosley, & Heger 2001) are also desired. Poynting flux produced from within such engines is a leading candidate to power GRB. The predicted variability on time scales ~ 1 s, based on the relative phase of toroidal and poloidal fields in our dynamo cycle, suggests an analogous variability in Poynting-flux dominated GRB models.

Future work specifically on transient dynamo theory should also include self-consistent treatments of buoyancy losses (e.g. Cline, Brummell, & Cattaneo 2003) radial and latitudinal spatial dependence of the system, latitudinal differential rotation, dynamical treatments of the backreaction incorporating magnetic helicity conservation (e.g. Blackman & Field 2002; Brandenburg & Sandin 2004). Distinguishing the relative roles of the MRI, convection driven dynamos, and possibly shear-current effect dynamos (Rogachevskii & Kleeorin 2003) also warrants further work. The extent to which the MRI might require latitudinal, rather than radial shear in the pressure supported interior of a star is of particular interest. The MRI in such environments has thus far been studied only in the linear regime (Balbus & Hawley 1994).

Acknowledgments: EGB acknowledges support from NSF grant AST-0406799, NASA grant ATP04-0000-0016, and the KITP of UCSB, where this work was supported in part by NSF Grant PHY-9907949. JTN acknowledges a Horton Fellowship from the Laboratory for Laser Energetics. JHT was supported in part by a Senior Visiting Fellowship at the Isaac Newton Institute for Mathematical Sciences, University of Cambridge, under EPSRC Grant N09176. Thanks to the referee for inducing our inclusion of the nonlinear shear evolution.

REFERENCES

Akiyama, S., Wheeler, J. C., Meier, D. L., & Lichtenstadt, I. 2003, ApJ, 584, 954

Ardeljan, N. V., Bisnovatyi-Kogan, G. S., & Moiseenko, S. G. 1998, Lecture Notes in Physics (Berlin: Springer Verlag), 506, 145

Balbus, S. A. & Hawley, J. F. 1994, MNRAS, 266, 769

Balbus, S. A. & Hawley, J. F. 1998, Rev. Modern Phys., 70, 1

Blackman, E. G. & Field, G. B. 2000, MNRAS, 318, 724

Blackman, E. G., Frank, A., Markiel, J. A., Thomas, J. H., & Van Horn, H. M. 2001, Nature, 409, 485

Blackman, E. G. & Brandenburg, A. 2003, ApJ, 584, L99

Blackman, E. G., & Field, G. B. 2002, Phys. Rev. Lett., 89, 265007

Blackman, E. G. & Field, G. B. 2004, Phys. of Plasmas, 11, 3264

Blackman, E. G., & Tan J.C. 2004, in Proceedings of the International Workshop on Magnetic Fields and Star Formation: Theory vs. Observation (Dordrecht: Kluwer), A. I. Gmez de Castro et al. eds, astro-ph/0307455

Braithwaite J. & Spruit H.C. 2004, Nature 431, 819.

Brandenburg, A., Nordlund, A., Stein, R. F., & Torkelsson, U. 1995, ApJ, 446, 741

Brandenburg, A., & Sandin, C., 2004, Astron. Astrophys. 427, 13-21

Brandenburg, A., Subramanian K., 2004, Phys. Rep. in press, 2004, astro-ph/0405052.

Charbonneau, P. & MacGregor, K. B. 1997, ApJ, 486, 502

Cline, K. S., Brummell, N. H., & Cattaneo, F. 2003, ApJ, 599, 1449

Cobb, B. E., Bailyn, C. D., van Dokkum, P. G., Buxton, M. M., & Bloom, J. S. 2004, ApJ, 608, L93

Durney, B.R., & Robinson, R.D. 1981, ApJ, 253, 290

Gal-Yam, A., et al. 2004, ApJ, 609, L59

Galama, T. J., et al. 1998, Nature, 395, 670

Heger, A., Langer, N., & Woosley, S. E. 2000, ApJ, 528, 368

Herant, M., Benz, W., Hix, W. R., Fryer, C. L., & Colgate, S. A. 1994, ApJ, 435, 339

Hjorth, J., et al. 2003, Nature, 423, 847

Iwamoto, K., et al. 1998, Nature, 395, 672

Khokhlov, A. M., Höflich, P. A., Oran, E. S., Wheeler, J. C., Wang, L., & Chtchelkanova, A. Y. 1999, ApJ, 524, L107

Leblanc, J. M. & Wilson, J. R. 1970, ApJ, 161, 541

Lai, D. & Qian, Y. 1998, ApJ, 505, 844

MacFadyen, A.I. & Woosley S.E. 1999, ApJ, 524, 262

MacFadyen, A. I., Woosley, S. E., & Heger, A. 2001, ApJ, 550, 410

Malesani, D., et al. 2004, ApJ, 609, L5

Markiel, J.A., Thomas, J.H., & Van Horn, H.M. 1994, ApJ, 430, 834

Markiel, J. A., & Thomas, J. H. 1999, ApJ, 523, 827

Matt, S., Frank, A., & Blackman, E. G. 2004, ASP Conf. Ser. 313: Asymmetrical Planetary Nebulae III: Winds, Structure and the Thunderbird, 449

Meier, D. L., Epstein, R. I., Arnett, W. D., & Schramm, D. N. 1976, ApJ, 204, 869

Moiseenko, S. G., Ardeljan, N. V., & Bisnovatyi-Kogan, G. S. 2003, Revista Mexicana de Astronomia y Astrofisica Conference Series, 15, 231

Moiseenko S.G., Bisnovatyi-Kogan G.S., Ardeljan N.V. 2004, *Magnetorotational supernova simulations*, in "1604-2004 Supernovae as Cosmological Lighthouses" (San Francisco: ASP), astro-ph/0410330

Parker, E. N. 1955, *ApJ*, 121, 491

Parker, E. N. 1979, *Cosmical Magnetic Fields* (Oxford: Clarendon Press)

Parker, E. N. 1993, *ApJ*, 408, 707

Robinson, R.D., & Durney, B.R. 1982, *A&A*, 108, 322

Rogachevskii & Durney, B.R. 1982, *Phys. Rev.E.*, 68, 036301

Stanek, K. Z., et al. 2003, *ApJ*, 591, L17

Thomas, J. H., Markiel, J. A., & Van Horn, H.M. 1995, *ApJ*, 453, 403

Thomsen, B., et al. 2004, *A&A*, 419, L21

Thompson, C. & Duncan, R. C. 1993, *ApJ*, 408, 194

Vishniac, E. T., & Cho, J. 2001, *ApJ*, 550, 752

Wheeler, J. C., Yi, I., Höflich, P., & Wang, L. 2000, *ApJ*, 537, 810

Wheeler, J. C., Meier, D. L., & Wilson, J. R. 2002, *ApJ*, 568, 807

Wheeler, J. C. 2004a, “3-D Explosions: A Meditation on Rotation (and Magnetic Fields)” in *Cosmic Explosions in Three Dimensions: Asymmetries in Supernovae and Gamma-Ray Bursts*, eds. P. Höflich, P. Kumar and J. C. Wheeler, (Cambridge: Cambridge University Press), astro-ph/0401322.

Wheeler, J. C. 2004b, “Conference Summary: Three Dimensional Explosions” in *Cosmic Explosions in Three Dimensions: Asymmetries in Supernovae and Gamma-Ray Bursts*, eds. P. Höflich, P. Kumar and J. C. Wheeler, (Cambridge: Cambridge University Press), astro-ph/0401323

Woosley, S. E., Heger, A., & Weaver, T. A. 2002, *Reviews of Modern Physics*, 74, 1015

Yoshimura, H. 1975, *ApJS*, 29, 467

Zhang, K., Chan, K. H., Zou, J., Liao, X., & Schubert, G. 2003, *ApJ*, 596, 66

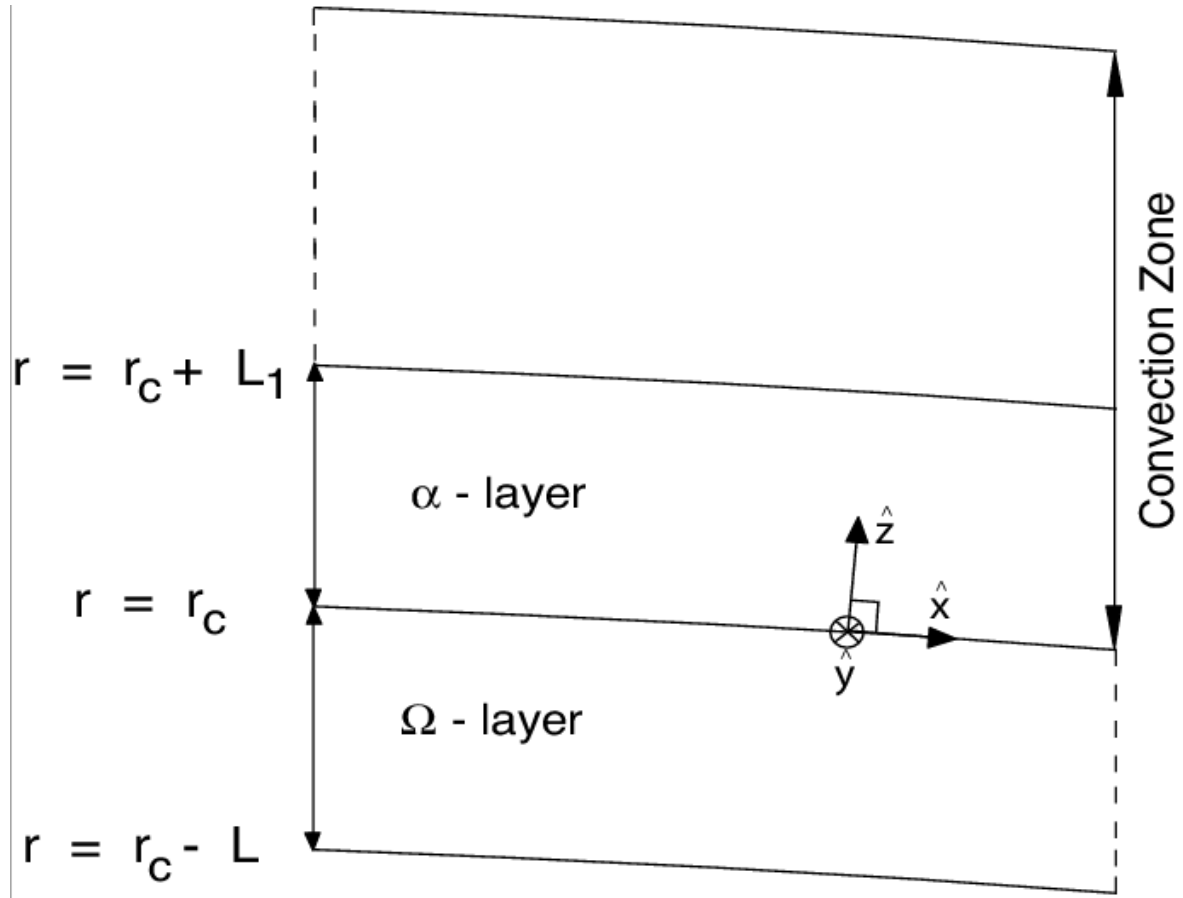


Fig. 1.— Schematic meridional slice of the spherical dynamo engine. The local Cartesian coordinate system is shown. The α -effect occurs in a layer of thickness L_1 equal to the local density scale height at the base of the convection zone ($r = r_c$). The Ω -effect occurs in a concentrated region of thickness L which extends from the surface of the NS to the base of the convection zone.

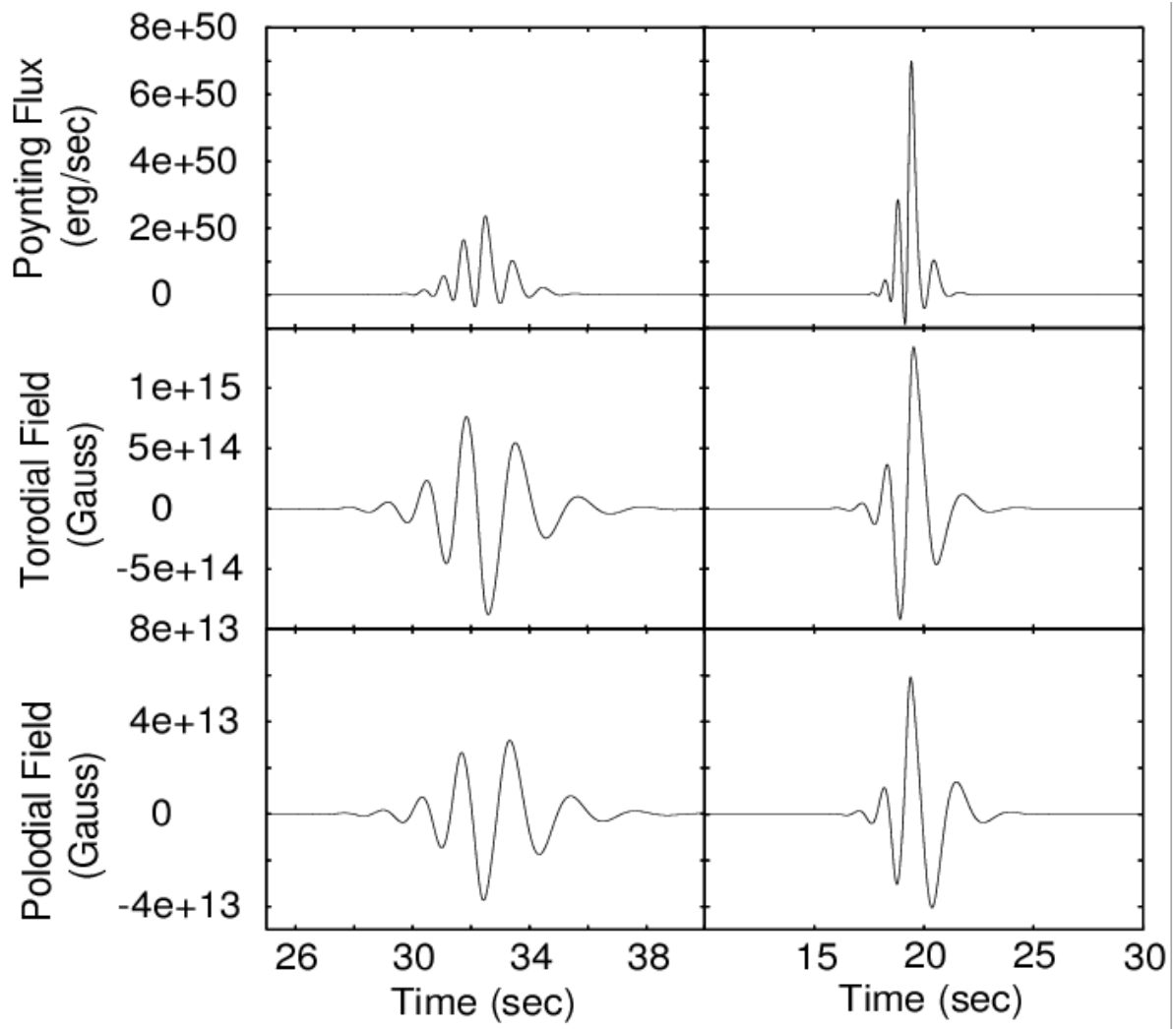


Fig. 2.— Toroidal and poloidal field strengths are shown for various values of Ω_0 and $\Delta\Omega_0 = f_0\Omega_0$. The figures on the left correspond to $\Omega_0 = 160$ Hz and $f_0 = 0.7$ while the figures on the right are for $\Omega_0 = 200$ Hz and $f_0 = 0.6$. The time from growth to decay of the fields is ~ 10 s in each case.

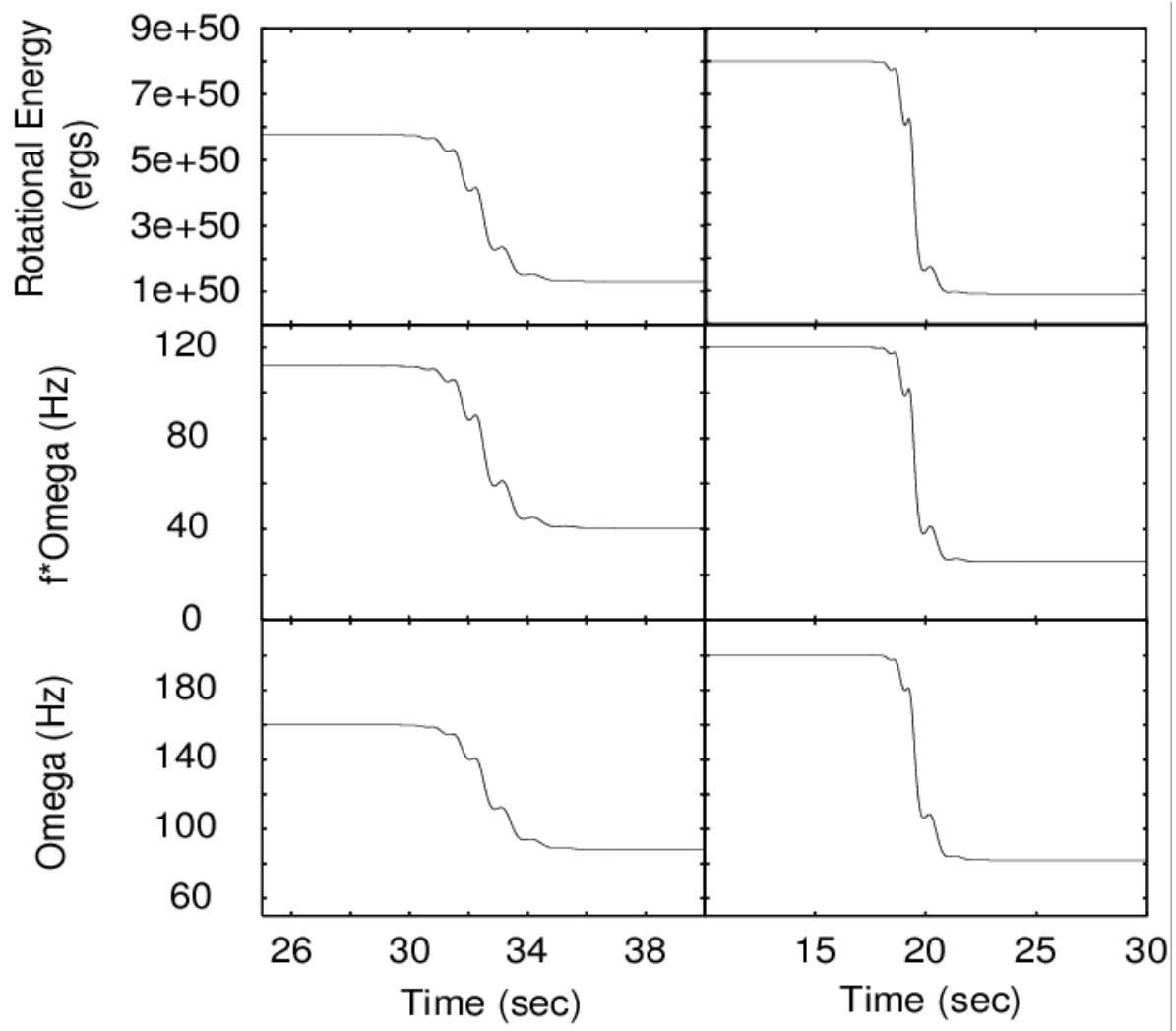


Fig. 3.— Time evolution of $\Omega(t)$, $\Delta\Omega(t)$, and $E(t)$. Similar to Fig. 2 with the left column corresponding to $\Omega_0 = 160$ Hz and $f_0 = 0.7$ and the right corresponding to $\Omega_0 = 200$ Hz and $f_0 = 0.6$. The rotational energy is drained through field generation until the dynamo number, N_D falls below 1, at which point the fields begin to decay.

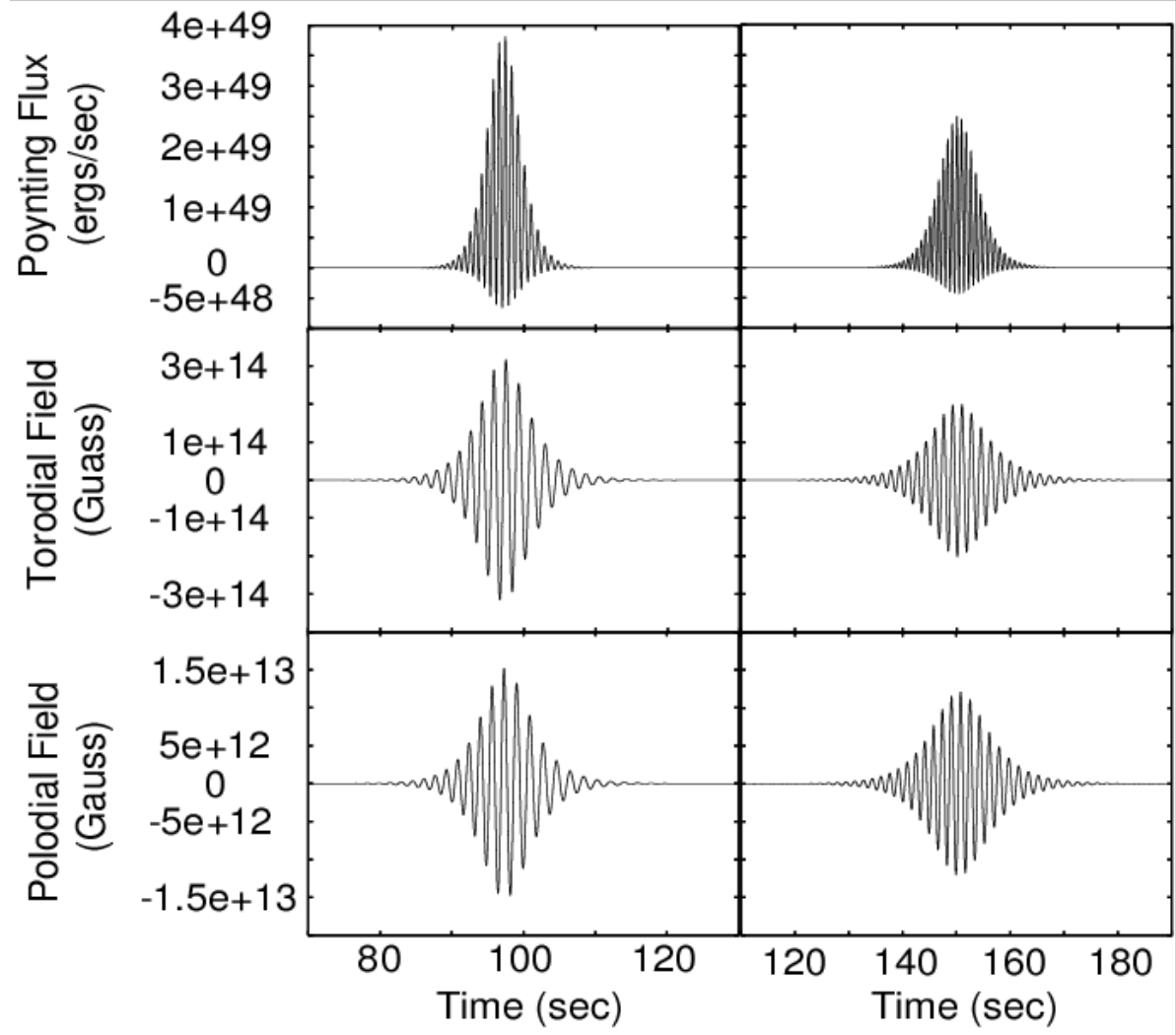


Fig. 4.— Toroidal and poloidal field strengths are shown for various values of Ω_0 and $\Delta\Omega_0 = f_0\Omega_0$. The figures on the left correspond to $\Omega_0 = 160$ Hz and $f_0 = 0.5$ while the figures on the right are for $\Omega_0 = 200$ Hz and $f_0 = 0.3$. The time from growth to decay of the fields is ~ 40 s in each case resulting in more field cycles during the lifetime of the dynamo when compared to Fig 1.

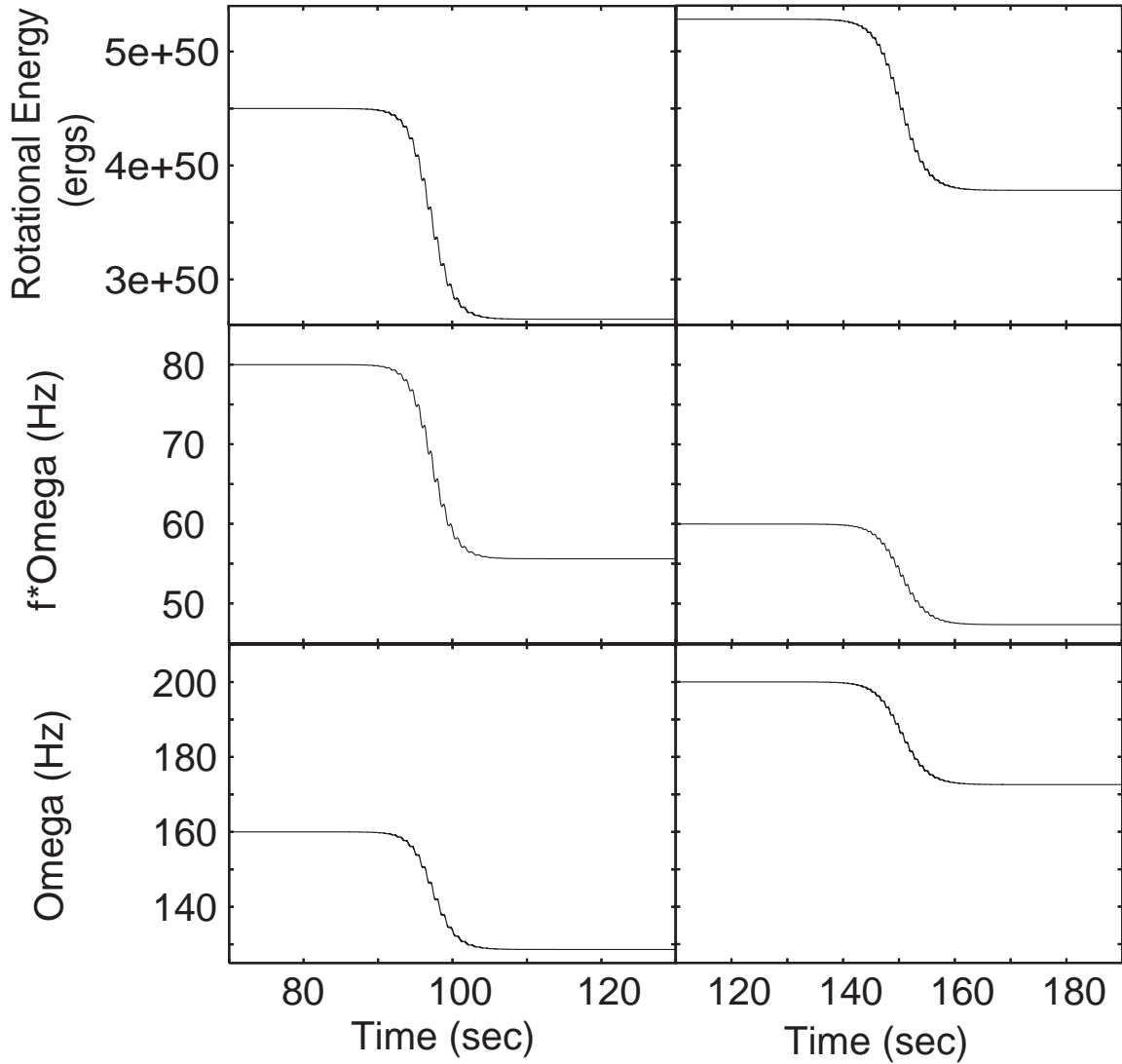


Fig. 5.— Time evolution of $\Omega(t)$, $\Delta\Omega(t)$, and $E(t)$. Similar to Fig. 2 with the left column corresponding to $\Omega_0 = 160$ Hz and $f_0 = 0.5$ and the right corresponding to $\Omega_0 = 200$ Hz and $f_0 = 0.3$.

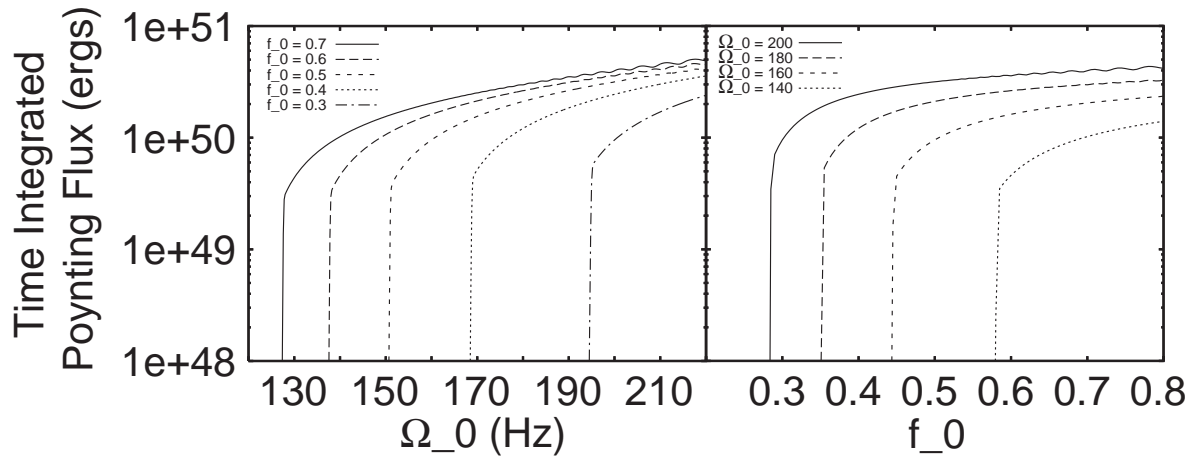


Fig. 6.— Time integrated Poynting flux for a range of initial Ω_0 , and f_0 values. Stronger shear and rotation lead to larger Poynting fluxes.